Structural Properties of the Multiwall Carbon Nanotubes/Poly(Methyl Methacrylate) Nanocomposites: Effect of the Multiwall Carbon Nanotubes Covalent Functionalization

Danijela V. Brković,[1] Vladimir B. Pavlović,[2,3] Vera P. Pavlović,[4] Nina Obradović,[3] Miodrag Mitrić,[5] Sanja Stevanović,[6] Branislav Vlahović,[7] Petar S. Uskoković,[1] Aleksandar D. Marinković[1]

[1]*Faculty of Technology and Metallurgy, University of Belgrade, Belgrade, Serbia*

[2]*FoA, Department for Physics and Mathematics, University of Belgrade, Belgrade, Serbia*

[3]*Institute of Technical Sciences of the SASA, Belgrade, Serbia*

[4]*Faculty of Mechanical Engineering, University of Belgrade, Belgrade, Serbia*

[5]*Vinča Institute of Nuclear Sciences, University of Belgrade, Belgrade, Serbia*

[6]*ICTM, Institute of Electrochemistry, University of Belgrade, Belgrade, Serbia*

[7]*NASA University Research Center for Aerospace Device Research and Education and NSF Center of Research Excellence in Science and Technology Computational Center for Fundamental and Applied Science and Education, North Carolina*

The structural characteristics of polymer nanocomposites with functionalized multiwall carbon nanotubes (MWCNTs) in poly(methyl methacrylate) matrix have been studied in relation to nanofiller loading and surface functionality. Different functional groups have been covalently attached on the MWCNTs sidewalls in order to induce interfacial interactions at nanofiller/polymer interface, which resulted in an improved nanomechanical features. Structural properties of nanocomposites, studied with XRD and Raman analysis, indicated the most pronounced decrease in a degree of amorphousness for samples containing 0.5 and 1 wt% of MWCNTs functionalized with dapsone (dapson-MWCNT) and diethyl malonate (dem-MWCNT). SEM and TEM micrographs confirmed improved dispersibility of the MWCNTs modified with aromatic structure of dapsone inside PMMA matrix. A significant increase in a glass transition temperature of over 60°C has been found for the 1 wt% dapson-MWCNT nanocomposite. Additional modification of dapson-MWCNT by further increasing aromaticity and voluminosity of attached moiety (fid-MWCNT), showed 30°C increases in a glass transition temperature at 4 wt% of nanofiller loading, which is similar to shift of 37°C with loading of MWCNTs modified with ester terminal group. A maximum increase of 56% of reduced modulus and 86% of hardness was obtained for 1 wt% loading of dapson-MWCNT nanofiller. POLYM. COMPOS., 38:E472–E489, 2017.

Correspondance to: A. Marinković; e-mail: marinko@tmf.bg.ac.rs
Contract grant sponsor: Faculty of Technology and Metallurgy, University of Belgrade, Karnegijeva 4, Belgrade, Serbia (Project Nos. III45019 and 172057); contract grant sponsor: NSF; contract grant number: HRD0833184; contract grant sponsor: NASA; contract grant number: NNX09AVO7A.

Additional Supporting Information may be found in the online version of this article.

DOI 10.1002/pc.23996

Published online in Wiley Online Library (wileyonlinelibrary.com).

INTRODUCTION

Among the variety of materials, multiwall carbon nanotubes/poly(methyl methacrylate) (MWCNTs/PMMA) composites have been extensively investigated, on research levels as well as for commercial and industrial purposes. The immense potential of tailoring material properties, by varying the amount of fillers and methods of composite preparation render them as promising

materials in wide range of applications [1–3]. Outstanding physical properties of MWCNTs make them an excellent reinforcing agent within amorphous polymer matrix. The presence of MWCNTs drastically changes the features of the matrix in which they are dispersed and resulting material is substantially improved, enhancing its performance in terms of structural, thermal, electrical, and mechanical properties. In order to achieve uniform nanoscale distribution of the filler in the polymer matrix, different techniques for nanocomposite preparation have been applied, which includes *in situ* or *ex situ* polymerizations [4–6], utilization of surfactant [7], electrospinning [8], coagulation [9], solution mixing/casting, melt mixing [10, 11], and combination of solution casting and melt mixing [12]. The composites have been made as a freestanding films [13] as well as films deposited on the different substrates [14, 15]. Thin and thick nanostructured polymeric films have been prepared for a wide range of applications in different fields of technology such as a photonic devices [16], field emitters [14], and gas-sensing devices [17].

It is a well-established fact that widespread use of MWCNTs is limited by their tendency toward aggregations due to the strong intermolecular van der Waals interactions. Covalent functionalizations of the sidewalls of MWCNTs have proven to be an effective way to overcome solubility limitations and achieve homogeneous dispersion by improving interfacial adhesion of filler in the host polymer matrix. Although, this functionalization approach facilitates distribution of MWCNTs in a different media, distortion of the structure and defects on the sidewalls can be a consequence of significant conversion of sp^2 hybridized carbon atoms into sp^3 in the carbon nanotube lattice.

The different types of covalent functionalization of MWCNTs within PMMA have been reported, but oxidation of MWCNTs surface by conventional acid treatment has been the most frequently used [18, 19]. The approach based on He plasma treatment of MWCNT followed by exposure to NH_3 resulted in nitrogen containing functional groups on sidewalls of nanotubes incorporated in PMMA [20]. The conversion of carboxyl groups on the surface of MWCNTs to acyl chloride and hydroxyl functionalities and its subsequent esterification was performed in order to obtain azo initiator-anchored nanotubes [21]. A grafting procedure for carbon nanotubes modification was performed in order to increase their hydrophobicity. MWCNTs grafted by PMMA were synthesized *via* a microemulsion polymerization of methyl methacrylate (MMA) in the presence of acid-modified multiwalled carbon nanotubes [22]. A certain degree of hardness can be achieved by controlling the amount and type of functionalities of the reinforced material. Mammeri et al. studied influence of the surface chemistry on nanomechanical properties of nanocomposites through the use of diazonium salts. The resulting MWCNTs served as platform for the growth of PMMA brushes by atomic transfer radical polymerization (ATRP). Hybrid thin films, prepared by spin-coating demonstrated unambiguously that MWCNTs reinforce PMMA and improve mechanical properties of the resulting nanocomposites [23]. The same authors investigated the covalent grafting of hydrolyzable Si(OEt) groups on oxidized CNTs and noncovalent adsorption of a polycation in order to improve miscibility of MWCNTs inside PMMA matrices [24]. Nanoindentation derived mechanical properties at the nano/microscale of functionalized MWCNTs/PMMA composites were also examined [25]. The effective dispersion of MWCNTs resulted in a substantially improved mechanical performance of nanocomposite films [26].

The choice of the solvents and preparation technique predominantly affects the final nanocomposite properties. Slobodian et al. demonstrated that position of electrical percolation threshold of PMMA/MWCNTs composites prepared by solution casting method, depends on the solvent selected to dissolve PMMA [27]. Kim et al. prepared MWCNT/PMMA composites by a solution-casting method with pristine, acid-treated and UV/ozone-treated MWCNT. Composites with UV/ozone-treated nanotubes showed the lowest sheet resistance, indicating that this treatment does not cause any surface damage rather helping MWCNT dispersions [28]. Tripathi et al. studied orientation behavior and bonding nature of MCWNTs inside composite films thickness about 40 μm [29]. Choi et al. founded that MWCNTs in nanocomposites, fabricated by solvent casting technique, have been better dispersed in the matrix, compared with coagulation technique, indicating that the dispersion state of the MWCNTs depends on the preparation procedure [9].

In this study, three types of functionalized MWCNTs have been prepared and used for fabrication of modified-MWCNT/PMMA nanocomposites. Functionalization of nanotube sidewalls was performed in order to improve compatibility of nanofiller inside PMMA matrix and induce intermolecular interactions nanofiller/polymer chains. Incorporation/dispersion of the nanosized reinforcement into polymer matrix and film formation was performed by using ultrasonication/solution casting technique to obtain free-standing nanocomposite films. The structural, thermal, and nanomechanical properties of prepared films have been investigated and discussed in relation to MWCNTs content and sidewalls functionalities.

EXPERIMENTAL

MWCNTs (Sigma-Aldrich), prepared by a chemical vapor deposition (CVD) method, before modification were thermally treated at 1,200°C under nitrogen for 4 h. The purity of MWCNTs was more than 95% and the outer and inner diameters were 20–30 and 5–10 nm, respectively, the length between 5 and 200 μm and specific surface area 40–600 m^2/g. Commercially available PMMA (Acryrex® CM205, Taiwan) $M_w = 90{,}400$ g/mol was purchased from Chi Mei Corp. All other reagents,

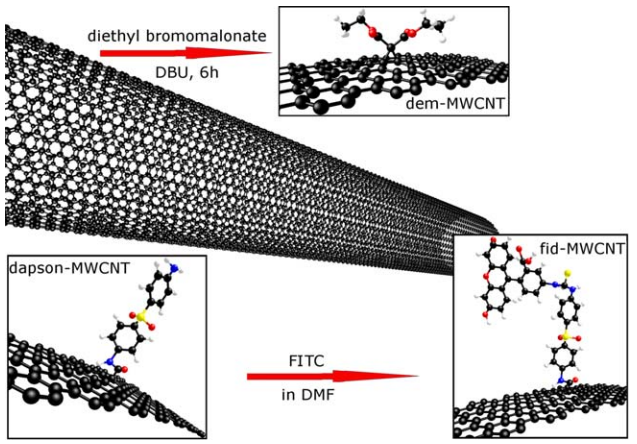

FIG. 1. The structures of functional groups on MWCNTs surfaces.

i.e., 4.4-diaminodiphenyl sulfone (dapsone), 1,8-diazabicyclo[5.4.0]undec-7-ene (DBU), diisopropyl amine (DIEA), *O*-(7-azabenzotriazol-1-yl)-*N*,*N*,*N*′,*N*′-tetramethyluroniumhexafluoro-phosphate (*N*-HATU), diethyl bromomalonate, concentrated sulfuric and nitric acid (H_2SO_4 and HNO_3), methanol, *N*,*N*-dimethylformamide (DMF), *N*-methyl-2-pyrrolidinone (NMP), and fluoroescein isothiocyanate (FITC) were used as received. Millipore, deionized (DI) water (18 MΩ cm resistivity) was used for sample washing and solution preparation. All chemicals were obtained from Sigma-Aldrich.

Preparation of Functionalized MWCNTs

Preparation of dem-MWCNT *via* Bingel reaction: 20 mg of MWCNTs were dispersed in 30 mL of 1,2-dichlorobenzene and sonicated for 15 min. The diethyl bromomalonate (3.52 mmol) and 1 mL of DBU were added to a suspension. This mixture was then sonicated for 6 h at 35°C in an ultrasonic bath, allowed to cool down to room temperature, filtered through a 0.05 μm PTFE membrane and washed with 50 mL of 1,2-dichlorobenzene and 200 mL of ethanol. Finally, the materials were dried in the vacuum drying oven at 60°C for 4 h and the desired products were obtained (Fig. 1)

Preparation of dapson-MWCNT and fid-MWCNT (Fig. 1) was performed according to previously established procedures [30]. In brief, o-MWCNT were prepared by treating the raw-MWCNT with a (3:1 V/V) mixture of concentrated H_2SO_4 and HNO_3, 3 h at 40°C in an ultrasonic bath, extensively washed with DI water until neutral the pH, and dried in a vacuum oven (80°C/8 h). A mixture of 300 mg o-MWCNT, 24 mg N-HATU, 30 μL DIEA (molar ratio N-HATU:DIEA was 1:3) and 9 mL anhydrous DMF was activated for 15 min, and after addition of dapsone dissolved in anhydrous DMF (60 g amine/300 mL DMF) the obtained dispersion was sonicated for 4 h at 40°C. The product was purified by washing with extensive quantity of DMF and methanol and dried in a vacuum oven at 60°C for 8 h. Conjugation of dapson-MWCNTs with FITC was achieved by mixing a solution of 50 mg of FITC and 50 mg of dapson-MWCNT in 30 mL of DMF and sonicated at room temperature for 5 h. After removal of the DMF, the black solid was dialyzed against H_2O for 3 days in a 12–14 K MWCO dialysis tube. Subsequently, the fid-MWCNT was isolated by lyophilization.

Preparation of MWCNT/PMMA Nanocomposites

Nanocomposite films (≈0.06-mm thick) were prepared by mechanical mixing of PMMA dissolved in chloroform and covalently modified MWCNTs dispersed in an appropriate solvent. PMMA was dissolved in chloroform by mechanical mixing at room temperature (500 rpm for 12 h). Stable dispersions of dapson- and fid-MWCNT were obtained in DMF, whereas dem-MWCNTs were dispersed in NMP. The mixtures were sonicated (at 40°C in an ultrasonic bath, Bandelin electronic, Berlin, Germany, power 120 W, frequency 35 kHz) for 5 min to help homogenization/de-agglomeration of the functionalized MWCNTs, followed by mechanical mixing at 500 rpm for the next 3 h. The resulting MWCNTs dispersion was added into PMMA solution and mechanically mixed at 500 rpm for the next 6 h to provide homogenous distribution inside polymer matrix. For preparation of free-standing composite films, the mold and a copper mask were used. The 30 μl of resulting mixture of PMMA and functionalized MWCNTs was drop-casted into a copper mask covering an area of 1 cm^2. After solvent evaporation the films were removed from the molds, separated from the copper mask, dried for 24 h on the air and 12 h on 40°C in a drying oven. Thick, homogeneous and transparent polymer/MWCNT nanocomposites having 0.5, 1, 2, and 4 wt% of the functionalized MWCNTs were obtained. Figure 2 shows a schematic representation of preparation process.

Characterization of MWCNT/PMMA Composites

Fourier-transform infrared (FT-IR) spectra were recorded in the transmission mode between 400 and 4,000 cm^{-1} using a BOMEM (Hartmann & Braun) spectrometer with a resolution of 4 cm^{-1}. X-ray diffraction (XRD) data were obtained using a BRUKER D8 ADVANCE with Vario 1 focusing primary monochromator (Cu $k_{\alpha 1}$ radiation, $\lambda = 1.54059$ Å). XRD patterns were obtained over the Bragg angle (2θ) range of 10°–50°.

Glass transition temperature T_g was investigated in a nitrogen atmosphere by the differential scanning calorimetry (DSC) method using SHIMADZU DSC-50 analyzer in the temperature region from room temperature to 180°C at a heating rate of 10°C min^{-1}. All the samples were heated from room temperature up to 180°C, cool-down to room temperature to erase any previous thermal

 DOI 10.1002/pc

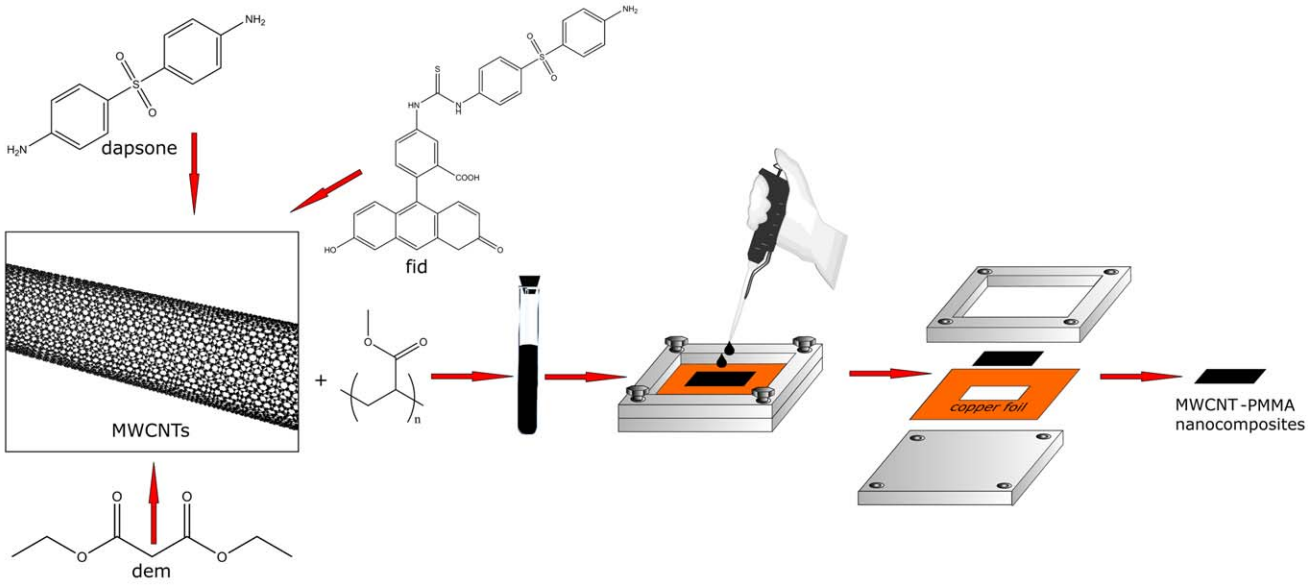

FIG. 2. Preparation of nanocomposites schematic representation.

history and heated again. The corresponding heating curves of the second cycle were recorded. The errors in temperatures are estimated to ±0.5°C, five samples of each formulations were tested.

Dispersion state of MWCNTs in the polymer has been viewed by scanning electron microscopy (SEM, model: JEOL JSM 6610LV). In order to study interfacial morphologies, the specimen films were frozen in liquid nitrogen and fractured to view matrix interface. Morphological characterization of the nanocomposite samples was performed on a transmission electron microscope (TEM) JEM-1400. The studying of coating morphology has been performed by NanoScope 3D (Veeco) microscope, which operated in tapping mode under ambient conditions. The agglomerate size dimension of functionalized MWCNTs on the surface of nanocomposite films was determined from AFM image profile line analysis.

Raman scattering was recorded using a Jobin-Yvon (Kyoto, Japan) U1000 system (spectrometer), in a back-scattering geometry. Unpolarized light scattering spectra of pure PMMA and nanocomposite films were obtained at room temperature using the 514.5 nm line of an Ar ion laser, with a 50 mW power. The laser beam was focused on a 5 lm spot size. The scanning range was 200–3,000 cm^{-1}.

The nanoindentation experiments on neat polymer films and MWCNT/PMMA nanocomposites were performed using a Triboscope T950 nanomechanical testing system (Hysitron, Minneapolis, MN) equipped with Berkovich indenter type with an *in situ* imaging mode. The frequently used power law method, developed by Oliver and Pharr [31] involves the extrapolation of a tangent to the top of the unloading curve to determine the depth (a combination of elastic and plastic displacement) over which the indenter is in contact with the specimen at the maximum load. A peak load of 2 mN was applied for all samples with a load-hold-unload of 20 s for each segment. Ten indentations were made for each sample and the average values and standard deviations are reported.

RESULTS AND DISCUSSION

FT-IR Analysis

In order to investigate structural properties of prepared nanocomposites, FT-IR spectrometry was employed. FT-IR spectra of functionalized MWCNT, dem-MWCNT, dapson-MWCNT, and fid-MWCNT were subject of our previous studies [30, 32]. FT-IR spectra of nanocomposites suggested the presence of some noncovalent interactions between PMMA matrix and nanofillers. The presence of the broad band at 3,257 cm^{-1} is due to —OH stretching vibrations. The absorption bands originating from PMMA are the dominant absorption bands in the FT-IR spectra. The absorption bands at 2,996, 2,953, and ~2,884 cm^{-1} are assigned to stretch mode of a C—H bond vibration (—CH_2, —CH_3) [33]. The most characteristic change is associated with two absorption bands at 1,730 and 1,690 cm^{-1} which were partially overlapped. A very intensive absorption band at 1,730 cm^{-1} is due to ester carbonyl group stretching vibrations (C═O bond). Absorption band at 1,691 cm^{-1} appears as a shoulder in the spectrum of pristine PMMA. These two absorption bands overlap and their relative heights changes to some extent by varying amount of MWCNTs. With the increase of the wt% of functionalized MWCNTs, the intensity

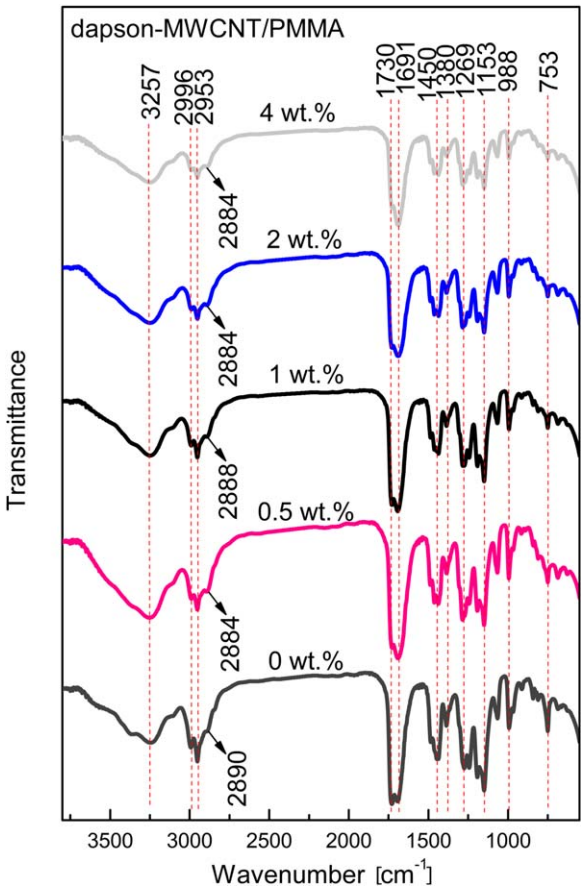

FIG. 3. FT-IR spectra of nanocomposite dapson-MWCNT/PMMA.

ratio of those absorption bands was changed in favor of the band at 1,691 cm^{-1} suggesting weak physical force rather than a strong chemical bonding between PMMA and nanotubes. Nonspecific interactions between dapsone molecule on the MWCNTs sidewalls and —COOH group of PMMA are probably formed *via* hydrogen bonding and π–π stacking. The band observed at ~1,450 cm^{-1} is attributed to band symmetric vibration of $—CH_2$. The absorption band at 1,380 cm^{-1} is attributed to bending vibrations of C—H bonds in $—CH_3$ groups. The bands characteristics for PMMA were observed [34]. The absorption bands at 1,192 and 1,153 cm^{-1} are due to the C—H deformations. The signal at 988 cm^{-1} is assigned to C—H in plane bending deformation. The C═O in-plane and out-of-plane bending are assigned to a band at 753 cm^{-1} [35]. Characteristic absorption bands mentioned above are observed in the FT-IR spectra of all prepared nanocomposites. Peaks originating from MWCNTs or functional groups on the surface of MWCNTs were not observed, probably due to overlapping with intensive PMMA signals. The only alteration in nanocomposite spectra, compared to pristine PMMA is in terms of relative heights changes and slight shifting of PMMA absorption bands. FT-IR spectrum of dapson-MWCNTs is shown in Fig. 3. FT-IR spectra of nanocomposites dem-MWCNT/PMMA and fid-MWCNT/PMMA are provided in Supporting Information file (Fig. S1).

XRD Analysis

The XRD patterns of neat PMMA and nanocomposites are shown in Figs. 4 and 5. The typical diffraction patterns of the amorphous polymer at the low 2θ values are obtained in spectra of all nanocomposites. Presented diffractograms revealed that all samples have a highly disordered amorphous structure. The ordering in the amorphous polymer structure (degree of amorphousness) can be determined by an arbitrary measure of the radial intensity distribution. The broader halo indicates high degree of disorder in polymer chains [36]. The first most intense peak at 2θ values for PMMA is observed at 12.80° and this signal refers to the distribution and ordering of PMMA chains, while the second, centered near to ~21° is due to the ordering within the main chains [37]. The second signal of neat polymer is, in this study, shifted to a lower 2θ value (at 15.78°) typical for amorphous polymers. This diffraction peak is shifted at around 21.0° in the case of samples containing MWCNTs, and in general, becomes narrow, indicating higher degree of ordering within MWCNT/PMMA nanocomposites.

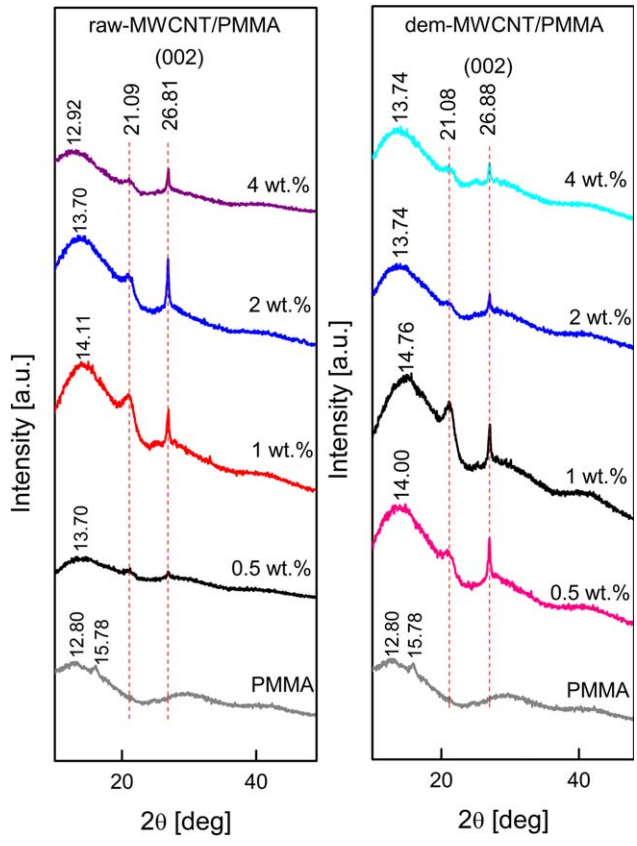

FIG. 4. XRD patterns of nanocomposites with different loadings of raw-MWCNT and dem-MWCNT.

DOI 10.1002/pc

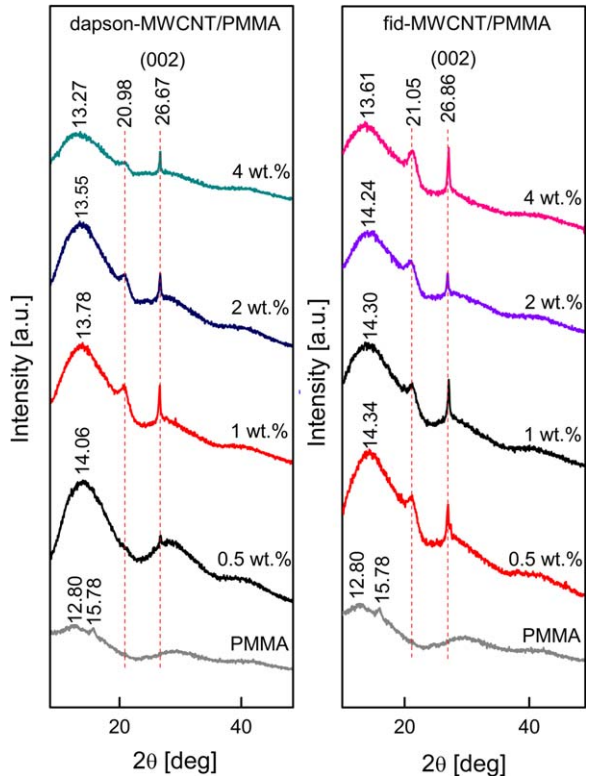

FIG. 5. XRD patterns of dapson-MWCNT/PMMA and fid-MWCNT/PMMA nanocomposites.

In Figs. 4 and 5 diffuse halos at lower 2θ values (at around 14°), assigned to PMMA, generally become narrower with addition of higher percent of functionalized MWCNTs in nanocomposite. This phenomenon is observed in XRD patterns of all prepared nanocomposites, suggesting significant contribution of MWCNTs to improved arrangement and ordering of PMMA chains. Addition of nanofillers caused substantial modification in the XRD patterns of PMMA observed in terms of additional peaks at 2θ ~26.8°. Diffraction signals corresponding to the ordered arrangement of the concentric cylinders of graphitic carbon MWCNTs walls are usually at around 26° (graphite indices of (0 0 2), *d*-value of 0.34 nm) [38]. In the case of raw and functionalized MWCNTs inside polymer matrix, characteristic peaks are slightly shifted toward higher 2θ value (at around 26.8°) which is clearly visible at Figs. 4 and 5. The intensity of 0 0 2 peaks depends from the amount and orientation of MWCNTs. The intensity increases with an increase in the MWCNTs volume and decreases when MWCNTs are horizontally aligned [39]. Atomic force microscopy (AFM) confirmed horizontal orientation of functionalized MWCNTs which resulted in an inconsistent intensity of 0 0 2 peaks with higher nanofiller loading. The impact on MWCNTs content and dispersion in polymer matrix, on the position, width and intensity of PMMA halos was investigated by calculating interplanar spacing (*d*) and interchain separation (*R*) in the PMMA network. The second diffraction signal, assigned to MWCNTs, at ~43° ($d = 0.208$ nm) is not observed in the XRD patterns, suggesting overlapping with the third peak of PMMA.

TABLE 1. XRD parameters for MWCNTs.

Sample	2θ (°)	*d*-spacing $d = \lambda/2 \sin\theta$ (Å)
raw-MWCNT/PMMA	26.81	3.323
dem-MWCNT/PMMA	26.88	3.314
dapson-MWCNT/PMMA	26.67	3.340
fid-MWCNT/PMMA	26.86	3.316

X-ray diffraction patterns also showed some structural changes in the molecular chain packing for all prepared nanocomposites. Figure 4 shows diffractograms of neat PMMA and nanocomposites with raw-MWCNT and dem-MWCNT. The degree of amorphousness is the highest within the neat PMMA, and then starts to decrease as the filler loading increases, until it reaches 2 wt%. The evident increase in a degree of amorphousness of the nanocomposites with 4 wt% of raw-MWCNT is probably due to bundling/aggregation and high content of unmodified MWCNTs, resulting in a different structure and orientation of polymer chains. Furthermore, Fig. 4 also presents XRD patterns of nanocomposites containing dem-MWCNT. The degree of ordering within the main chains (peak at 21.08°) is the highest for the sample with 1 wt% of dem-MWCNT indicating good arrangement of polymer chains.

The changes in XRD patterns of dapson-MWCNT/PMMA (Fig. 5) are also dependent from the concentration of the nanofiller. This peak at ~21° is absent only in the XRD pattern of the sample with 0.5% of dapson-MWCNT (Fig. 5) suggesting a lower degree of ordering within the main chains but exceptional improvement in ordered packing of polymer chains compared to diffractogram of neat PMMA. However, the effect of MWCNTs on degree of amorphousness of the polymer is inconsistent. Nanocomposites that contain 1 and 2 wt% of dapson-MWCNTs show an increase in intensity of diffraction peak and narrowing of a broad polymer signals at ~14° and 21°. The intensity of the signals belonging to polymer matrix for sample 0.5% fid-MWCNT/PMMA dramatically increased and thereafter remained almost constant with addition of a higher percentage of fid-MWCNT.

However, no considerable change in the peak position is observed, which reveals that the lattice parameters do not change significantly. Parameters given in Tables 1 and 2 confirmed this statement. The degree of amorphousness of PMMA matrix was reduced in the cases of all nanocomposites and improved alignment of macromolecular chains was achieved. This is particularly reflected in terms of nanomechanical properties, which will be described in more details.

TABLE 2. XRD parameters of neat PMMA and nanocomposites.

Sample	MWCNTs content (%)	2θ (°)	d-spacing $d = \lambda/2 \sin\theta$ (Å)	R (interchain spacing) $R = 5/8 (\lambda/\sin\theta)$ (Å)
PMMA	0	12.80	6.910	8.638
raw-MWCNT/PMMA	0.5	13.70	6.458	8.073
	1	14.11	6.272	7.839
	2	13.70	6.458	8.073
	4	12.92	6.846	8.558
dem-MWCNT/PMMA	0.5	14.00	6.321	7.901
	1	14.76	5.997	7.496
	2	13.74	6.440	8.049
	4	13.74	6.440	8.049
dapson-MWCNT/PMMA	0.5	14.06	6.294	7.867
	1	13.78	6.421	8.026
	2	13.55	6.530	8.162
	4	13.27	6.667	8.333
fid-MWCNT/PMMA	0.5	14.34	6.172	7.714
	1	14.30	6.189	7.736
	2	14.24	6.215	7.768
	4	13.61	6.501	8.126

Raman Analysis

Raman spectroscopy was used to provide further insight in the impact of the MWCNTs type and degree of functionalization on the properties of the nanocomposites. Raman spectra for the pristine PMMA and nanocomposite loaded with 0.5, 2, and 4 wt% of raw-MWCNT are shown in Fig. 6. There is an obvious appearance of the distinctive D and G bands in the spectra of all prepared nanocomposites. The G-band represents the intrinsic characteristics of carbon nanotubes, tangential Raman feature regarding vibrations of sp^2-bonded carbon atoms in a rolled-up graphitic layer of MWCNTs [40]. The intensity, shape, and the position of the D-band in graphite represents scattering from a defect in the symmetry of the graphene sheet, due to the presence of impurities or other symmetry-breaking defects. The intensity of the D-band is particularly important parameter since the ratio between D-band and G-band (I_D/I_G) provides information on graphitic lattice disorder [41–48].

The D-band is observed at around ~1,326 cm^{-1} in the nanocomposite sample containing 0.5 wt% of raw-MWCNT, while G band appears to be between two peaks: at 1,589 cm^{-1} and at ~1,606 cm^{-1} (centered at around ~1,595 cm^{-1}). A shoulder at ~1,613–1,619 cm^{-1} can be attributed to the D′ band. The G band, for a graphene sheet can be only seen as a one Lorentzian single peak at 1,582 cm^{-1}, whereas in SWCNT Raman spectra, G band can be observed as a complex with multiple peaks because of the curvature of the cylindrical SWCNT [49]. Although the G band in the SWCNT spectrum will consist of more than one peak (up to six), the two main signals can be distinguished: one at ~1,590 cm^{-1} (G^+) and second at about ~1,570 cm^{-1} (G^-). G^+ band modes are related to the vibrations of the carbon atoms along the nanotube axis and G^- band modes refer to the vibrations of carbon atoms along the circumferential direction. Considering that G band modes have high sensitivity to tube diameter distribution, the Raman features of the nanotubes with large diameters (MWCNTs) are closer to the features of graphite. An appearance of one G band, or G^+/G^- splitting in small intensity in the spectrum of MWCNTs, is due to effect of different diameter of concentric multiple rolled layers of graphene and variation between different nanotubes in an ensemble [49, 50]. The frequency of G band increases with decreasing diameter of nanotubes (for nanotubes with outer diameter ~70 nm is expected to be at ~1,580 cm^{-1}). For outer diameter of MWCNTs used in this study (~30 nm), shifting of G band to higher frequencies was anticipated. D′ band in Raman spectrum is caused by symmetry breaking of microscopic sp^2-crystallite size and appears in spectrum

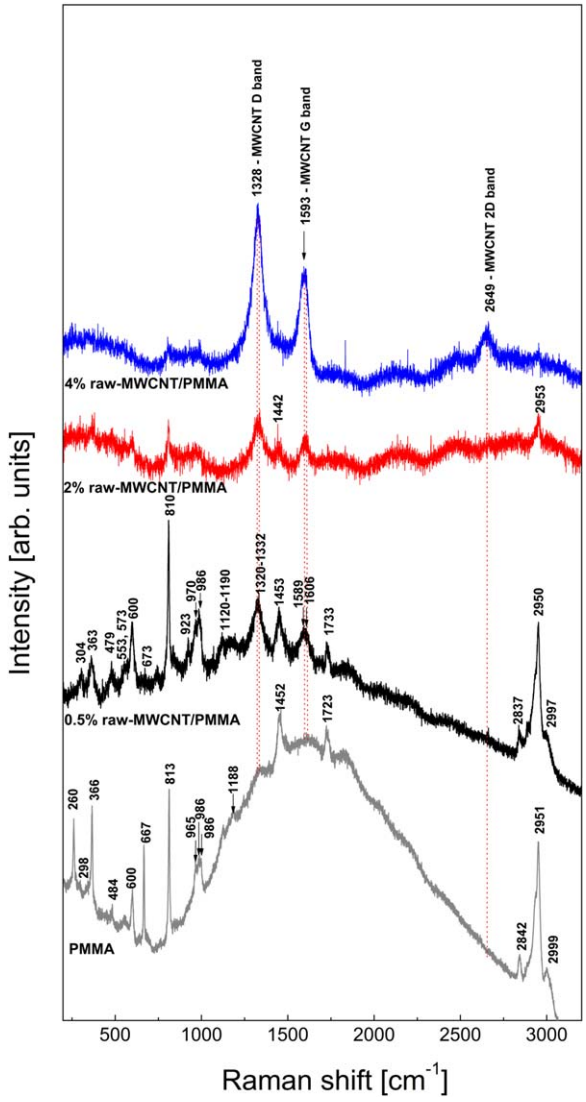

FIG. 6. Raman spectra of neat PMMA and raw-MWCNT/PMMA.

DOI 10.1002/pc

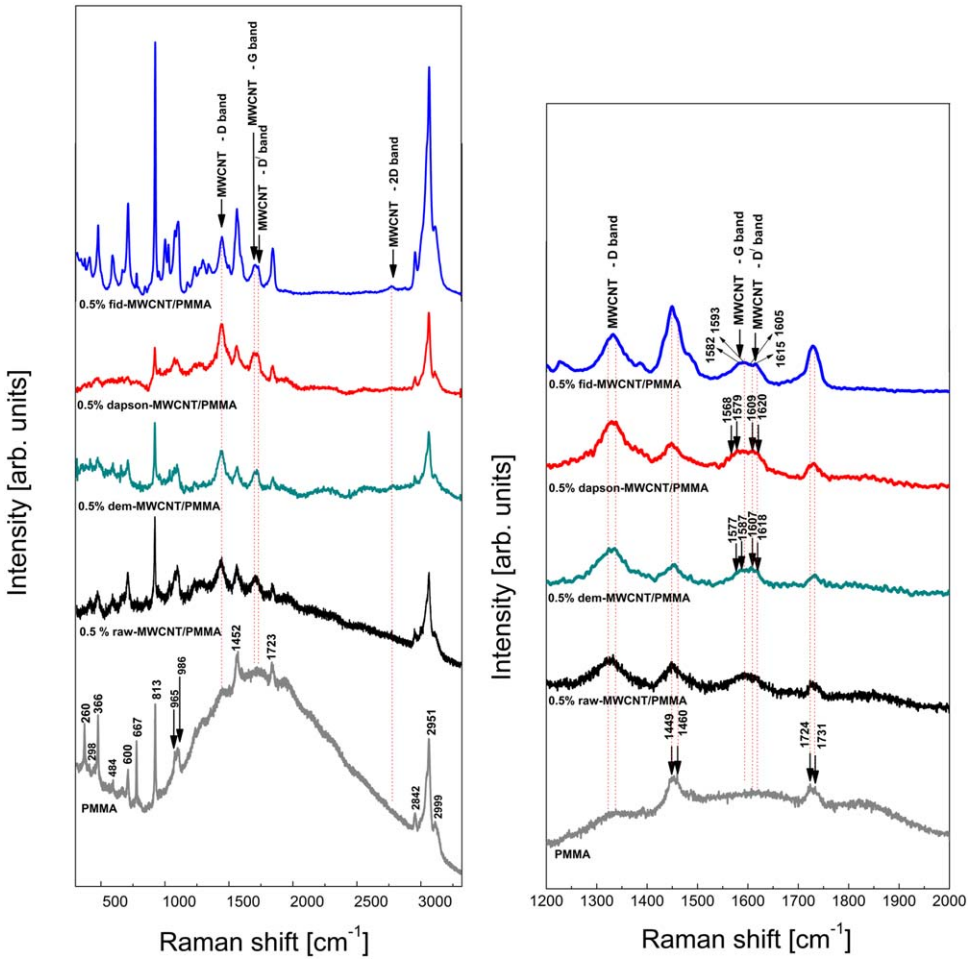

FIG. 7. Raman spectra of the nanocomposites containing 0.5 wt% of modified-MWCNTs.

as a low intensity shoulder on the G band, shifted toward higher frequencies (1,600–1,624 cm^{-1}) [51–57].

It is a well-established fact that D and D′ bands are closely related due to double resonance effect, which is associated with elastic phonons scattering close to K and Γ point of the graphite Brillouin zone. The G′ band (equivalent to the 2D overtone) is caused by an inelastic phonon emission process [51, 56]. McClory et al. reported the existence of a relatively intense D band in CVD produced tubes, which clearly imply the high levels of defects sites even in as-produced nanotubes [10]. Considering that intensity of D and G bands is directly proportional to the number of sp^2 and sp^3 hybridized carbon atom, respectively, the I_D/I_G ratio is used for quantification of the defects in spectrum [51]. The position and intensity of the D band strongly depends on laser excitation energies and higher excitation energies shift D band toward lower frequencies [58]. The intensity of the D band in Raman spectrum of pure nanotubes (with minimum defects), for laser excitation wavelength of 457.9 nm, is always lower, compared to intensity of the G band [58]. However, when laser excitation wavelength is 514.5 nm, the intensity of the D band will be lower or close to the G band intensity, depending on the diameter of the nanotubes [41, 59]. If applied laser excitation wavelengths are higher (780, 830, and 1,064 nm), the intensity ratio will be reversed. From Raman spectra of the pure CNTs and CNTs inside PMMA matrix at similar wavelength used in thus study (~633 nm), I_D/I_G ratio was found to be in some cases $I_D/I_G > 1$, while in others $I_D/I_G < 1$ [40, 51, 60, 61]. The absence of the low frequency bands (100–300 or 200–400 cm^{-1}), characteristic for SWCNTs and DWCNTs due to the *radial breathing mode* is expected, especially considering that inner tube diameter of the used MWCNT is >2 nm [55]. Detailed analysis of raw-MWCNT/PMMA spectra is provided in Supporting Information file.

Figure 7 presents Raman spectra of nanocomposites with the same content (0.5 wt%) of functionalized MWCNTs. The bands originating from both polymer and nanofiller for sample 0.5% raw-MWCNT/PMMA have been described above. The addition of dem-MWCNT to polymer matrix instead of raw-MWCNT, resulted in a slightly intensity increase of all MWCNTs signals.

Although, Raman spectrum of the nanocomposite 0.5% dem-MWCNT/PMMA appears to be similar to the one with 0.5 wt% of the raw-MWCNT, changes of the D/G ratio in favor of D band were observed. The change in intensity of the D band indicates conversion of carbon atom from primarily sp^2-bonded to sp^3-bonded [53], thus confirming the successful covalent sidewall functionalization. The G peak splitting with a maximum on ~1,607 cm^{-1} and a shoulder corresponding to the D′ band at ~1,618 cm^{-1} in the Raman spectrum were also noticed.

Due to the addition of 0.5% dapson-MWCNT to PMMA matrix, MWCNTs Raman signals become even more pronounced, particularly up to the 1,210 cm^{-1}. The I_D/I_G ratio is increased, compared to dem-MWCNT/PMMA, suggesting that a higher degree of modification was achieved. The maximum of the G band is between 1,579 and 1,611 cm^{-1}, while the D′ band is observed at around 1,618 cm^{-1}.

The nanocomposites with 0.5% fid-MWCNT demonstrated an opposite trend, PMMA signals became dominant in the spectrum. The contribution of 2D band in the spectrum at 2,665 cm^{-1} is barely noticeable. The bands at 888 and ~ 914 cm^{-1} are assigned to PMMA and these signals were not observed in PMMA filled with dapson-MWCNT. The higher degree of ordering in the amorphous polymer structure, due to interaction of fid functional groups on the MWCNTs surface and polymer chains caused the appearance of the new PMMA signals. The I_D/I_G ratio is found to be similar to the one obtained for polymer filled with dapson-MWCNT which was expected, considering that dapson-MWCNT was used for further functionalization with FITC in order to obtain fid-MWCNT. The G peak splitting is less pronounced, although the broadness suggests that G peak is composed of several subpeaks. A shoulder at about ~1,615–1,617 cm^{-1} on the right side of G band, corresponding to the D′ signal is observed.

Raman spectra of nanocomposites with the same loading (2 wt%) of differently functionalized MWCNTs are shown in Fig. 8. The addition of 2% dem-MWCNT does not cause significant changes of Raman signals, with regard to the nanocomposite containing 2 wt% of raw-MWCNTs. The stronger MWCNTs bands and the slight increase of the I_D/I_G ratio for 2% dem-MWCNT/PMMA nanocomposite are the only evident differences. The continued increase of the MWCNTs signals with addition of 2 wt% of dapson-MWCNTs in polymer matrix is in accordance with results obtained for the nanocomposites containing 0.5 wt% functionalized MWCNTs. Clearly, visible 2D band is placed at ~2,654 cm^{-1}. The dominant signals in nanocomposite containing 2 wt% of fid-MWCNT are signals attributed to PMMA matrix. Contribution of the 2D band at 2,665 cm^{-1} in the case of 2% fid-MWCNT/PMMA is very weak and I_D/I_G ratio slightly increases. This increase, related to the changes in hybridization from sp^2 to sp^3 and creation of the surface defects

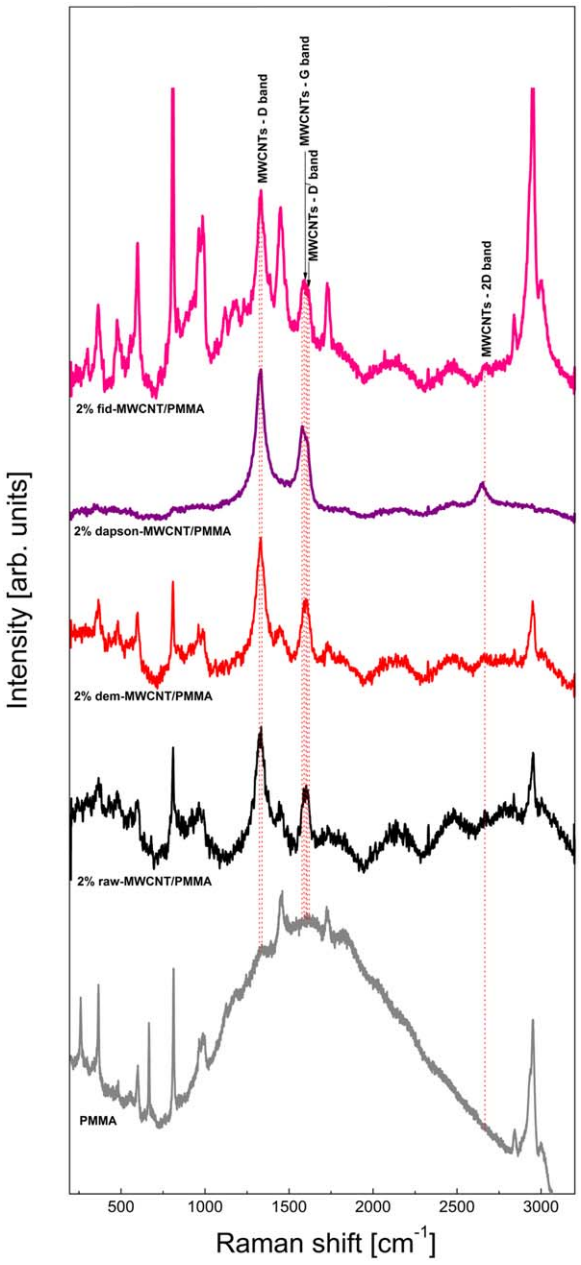

FIG. 8. Raman spectra of the nanocomposites with 2 wt% of modified-MWCNTs.

is not observed when addition of fid-MWCNT was lower (0.5 wt%).

The nanocomposites containing 4 wt% of the functionalized MWCNTs, as shown in Fig. 9, demonstrated significantly sharper G and D bands, compared with the spectra of the nanocomposites having lower loadings of carbon nanotubes. The G band complex is composed of the multiple peaks and can be observed at around 1,582–1,608 cm^{-1}. The peak at ~1,327 cm^{-1} corresponds to maximum of the D band, while the broad G′ band is placed at 2,649 cm^{-1}. The I_D/I_G ratio remains >1. Altogether, Raman peaks associated with the nanotubes dominate in the spectra of the nanocomposites containing 4

DOI 10.1002/pc

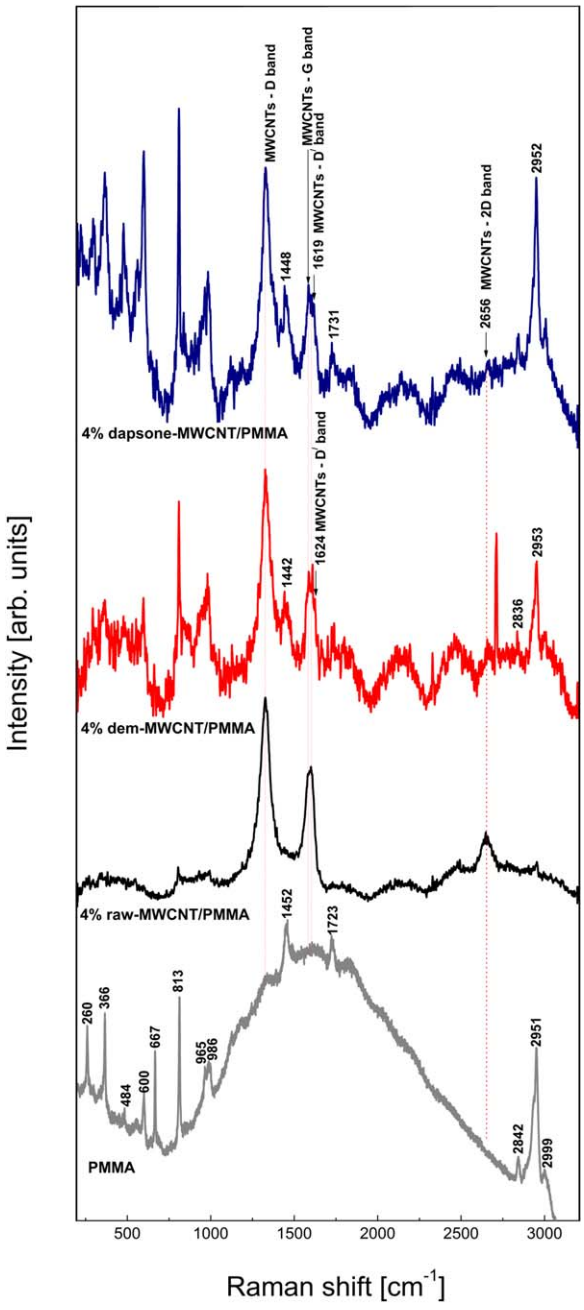

FIG. 9. Raman spectra of the nanocomposites containing 4 wt% of modified-MWCNT.

wt% of the functionalized MWCNTs. The degree of ordering in the polymer structure of these nanocomposites, having high weight percentages of functionalized carbon nanotubes decreased. The splitting of the G band in the nanocomposite sample with 4 wt% of the dem-MWCNT is quite distinct and more pronounced from the nanocomposites with unmodified MWCNTs. The shoulder on the right side (at $\sim$1,624 cm^{-1}) is attributed to the D′ band, whose presence is related to a higher degree of structural disorder. The existence of D′ band is in accordance with the change of D/G ratio in favor of D band, with regard to nanocomposites containing 4 wt% of unmodified MWCNTs. The decrease of 2D peak intensity is observable ($\sim$2,656 cm^{-1}), although is followed by the increase of the peak at 2,711 cm^{-1} typical for the amorphous carbon. The Raman bands with slightly higher intensity, originating from the polymer matrix are noticed on the following frequencies: $\sim$809, 980, and 2,953 cm^{-1}. The PMMA bands at $\sim$366, 597, and 1,442 cm^{-1} are less pronounced and the presence of low intensity bands at $\sim$661, 1,725–1,740, and 2,836 cm^{-1} is also observed. The addition of 4 wt% dapson-MWCNT instade of dem-MWCNT led to reduced Raman intensities of all MWCNTs bands. The intensity of those signals becomes comparable with the intensity of polymer signals. The I_D/I_G ratio increase with increasing functionalization degree (from dem-MWCNT to dapson-MWCNT). The signal assigned to D′ band for the sample 4% dapson-MWCNT/PMMA is observed at $\sim$1,619 cm^{-1}.

The results of Raman analysis of the dem-MWCNT/PMMA nanocomposites suggested the highest degree of ordering in the amorphous polymer structure for the nanocomposite samples 0.5% dem-MWCNT/PMMA and 1% dem-MWCNT/PMMA, considering that Raman signals of the polymer in these two spectra are the most distinct from the PMMA background signal. The I_D/I_G ratio primarily decreases with increasing dem-MWCNT content from 0.5% to 1%, and then starts to increase with higher content of dem-MWCNT (2 wt%), and once again decrease for the sample containing 4 wt% of dem-MWCNT.

The nanocomposites with dapson-MWCNT exhibit a different attenuation and the amplification of PMMA signals. For instance, samples containing 0.5 wt% dapson-MWCNT showed more intensive signals at 2,952, 1,448, and 1,731 cm^{-1}, in the range of 1,118–1,187 cm^{-1}, whereas the bands at lower frequencies (below 670 cm^{-1}) revealed decrease in signal intensity. The lowest degree of ordering in the amorphous polymer structure was observed for the sample 2 wt% dapson-MWCNTs/PMMA and the PMMA signals are attenuated. Similar to the samples with dem-MWCNT, we find that I_D/I_G ratio in dapson-MWCNT/PMMA as well as in fid-MWCNT/PMMA nanocomposites is not uniformly concentration-dependent function.

The highest degree of ordering in the amorphous polymer structure for the nanocomposite fid-MWCNT/PMMA was found for the sample 0.5% fid-MWCNT/PMMA. The G band for all concentration of fid-MWCNTs in those nanocomposites is composed of the multiple peaks, whereas the 2D band appears to be a broad Raman peak with very low intensity. Raman spectra of dem-MWCNT/PMMA and dapson-MWCNT/PMMA with different content of nanotubes loading are shown in Fig. 10.

Differential Scanning Calorimetry

DSC analysis was used to study the thermal properties of the MWCNT/PMMA composites. The glass transition

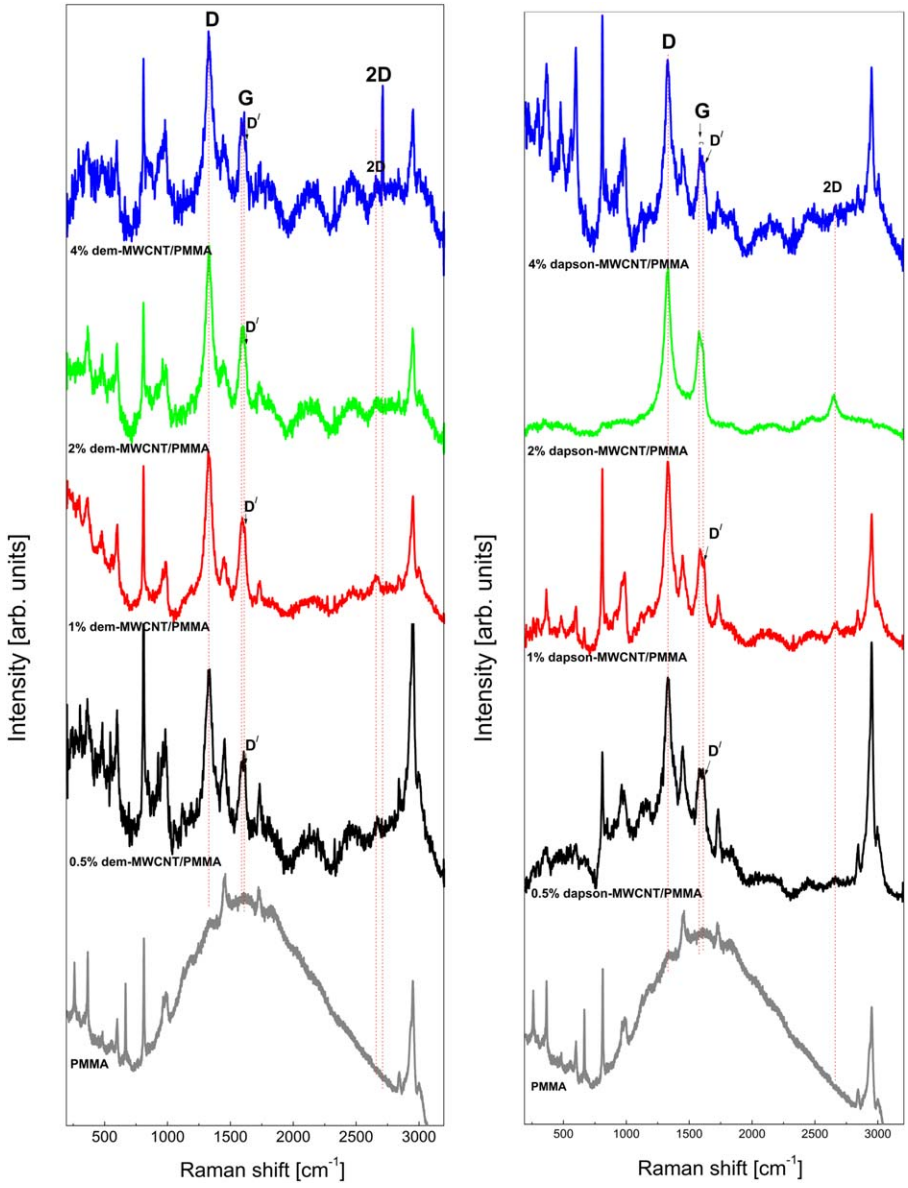

FIG. 10. Raman spectra of dem-MWCNT/PMMA and dapson-MWCNT/PMMA with different loadings of nanotubes.

temperatures (T_g) obtained from the DSC thermograms for neat PMMA as well as for MWCNT/PMMA composites with various MWCNTs contents are given in Table 3. The T_g observed by DSC analysis as an increase in the heat capacity of the sample during heating is caused by fragment motion in the PMMA chains [62]. It must be noted that even a trace amount of the unevaporated organic solvent in the samples prepared by solvent casting technique, causes shifting of T_g to the lower temperatures [62].

The gradual increase in T_g value with increasing MWCNTs content is observed for dem-MWCNT/PMMA and fid-MWCNT/PMMA nanocomposites indicating that main chain motion is restricted by increased presence of nanofiller. Agglomeration of unmodified nanotubes inside polymer at high MWCNTs contents (4 wt%), due to unequal distribution did not cause major constraint in PMMA chain motion. Regardless on that fact, a significant polymer-filler interaction led to reduction in the chain motion of the PMMA segments, reflected in increased T_g [63]. In the case of the composites containing fid-MWCNT, the optimal network structure, their uniform dispersion, good alignment, and restricted segmental motion of the PMMA chains was accomplished with the highest content of carbon nanotubes.

Otherwise, increases of T_g were also observed for nanocomposites with raw-MWCNT and dapson-MWCNT with nanofiller addition up to 2 and 1 wt%, respectively. The creation of the specific network structure of dapson-MWCNT with a low content (1 wt%) in PMMA,

TABLE 3. The results of DSC analysis.

Sample	MWCNTs content (%)	T_g (°C)	Q (J/g)
PMMA	0	66.91	−2.51
dapson-MWCNT/PMMA	0.5	64.97	−2.39
	1	130.48	−12.06
	2	73.84	−2.82
	4	69.61	−0.50
raw-MWCNT/PMMA	0.5	72.49	−1.39
	1	81.10	—
	2	84.44	−1.09
	4	72.05	−0.45
dem-MWCNT/PMMA	0.5	69.41	−1.30
	1	75.03	−1.42
	2	93.60	—
	4	104.35	−1.91
fid-MWCNT/PMMA	0.5	75.00	−1.13
	1	76.75	−1.13
	2	78.54	−1.35
	4	96.87	−5.04

probably had an impact on stronger restriction of mobility of the PMMA chains and caused exceptionally high T_g. Further increase in the content of dapson-MWCNT shows large decreases in T_g values, implying that optimal network structure and interfacial interactions were achieved for 1 wt% nanofiller addition. Strongly adsorbed polymer film with a layer thickness smaller than the radius of gyration of the chain behaves as a nonhomogeneous end-grafted dense network of polymer/nanofiller interactions. In a surrounding layers around nanofiller, the polymer have stretched configuration which, due to entropic elasticity, tends to compress the layer leading to a density higher than that of the bulk. The high grafting density, i.e., the number/intensity of polymer segments/nanofiller functionalities interactions will causes increase in T_g value. Obtained results clearly indicate that introduction of functionalized MWCNTs into PMMA polymer increased thermal stability of the polymer matrix.

SEM and TEM Analysis

The reinforcement mechanism of nanocomposites is efficient if the interfacial interaction between nanofiller and polymer matrix is strong. In such case, crack propagation tends to be inhibited due to increased toughness of reinforced nanocomposite. The SEM observations can qualitatively estimate extent of the interaction between the polymer matrix and MWCNTs. The study of dispersibility of nanotubes in PMMA has been performed on

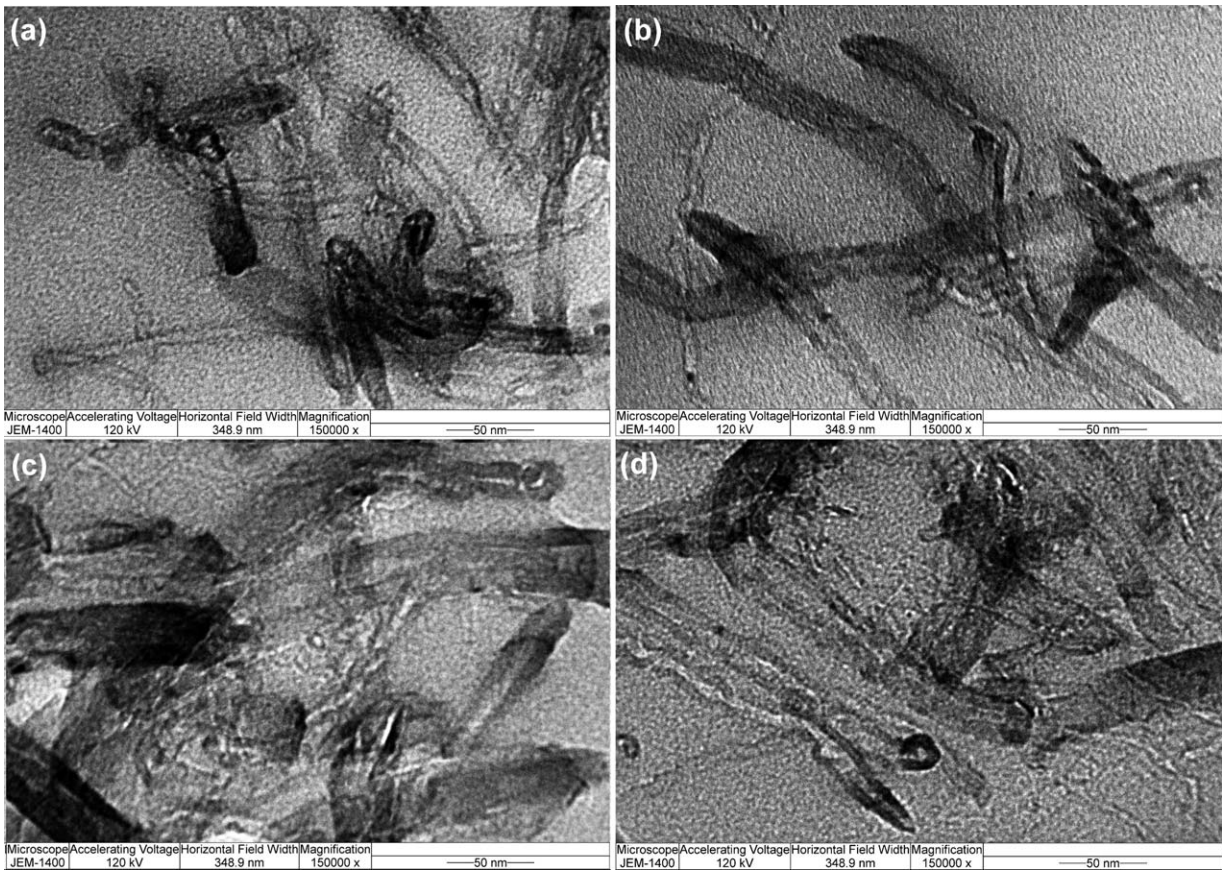

FIG. 11. TEM micrographs show the dispersion of 1 wt% MWCNTs load: (a) raw-MWCNT/PMMA, (b) dem-MWCNT/PMMA, (c) dapson-MWCNT/PMMA, and (d) fid-MWCNT/PMMA.

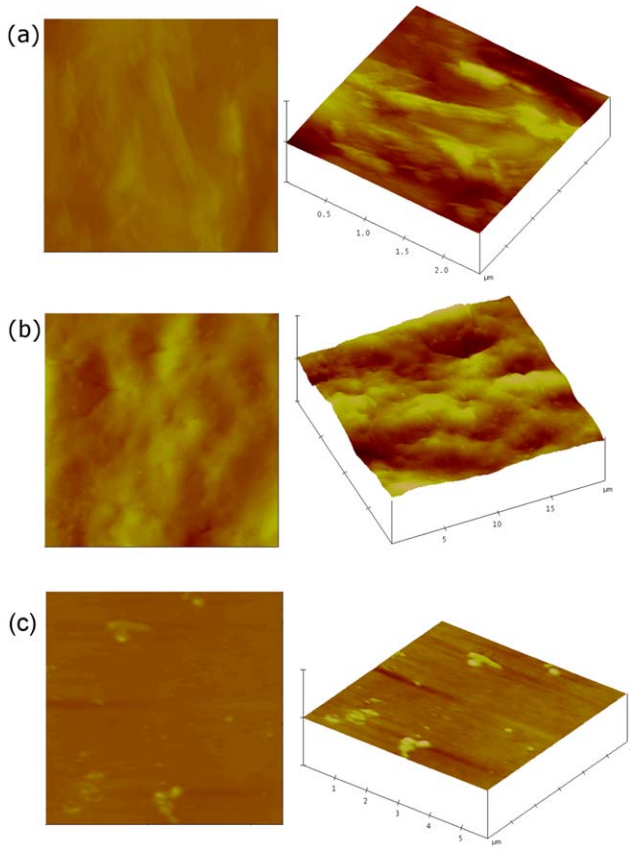

FIG. 12. AFM images of (a) neat PMMA film (2.5 × 2.5 × 1.5 μm), (b) nanocomposite with 0.5 wt% of dem-MWCNT (20 × 20 × 5 μm), and (c) 1 wt% of fid-MWCNT (5 × 5 × 0.3 μm).

fracture surfaces and composites of raw-MWCNT/PMMA, dem-MWCNT/PMMA, and dapson-MWCNT/PMMA with 1 wt% of nanofiller loadings was shown in Fig. S3. Poor dispersion and aggregation of raw-MWCNT was observed in PMMA (Fig. S3a), presumably due to complete removal of physically adsorbed oxygen-containing groups from MWCNTs surface during thermal treatment at 1,200°C. Exceptionally low wetting and imperfect interfacial adhesion between raw-MWCNT and the polymer matrix cause disruption of the continuity of polymer matrix with visible cavities (weakening point) which cause observable disintegration of nanocomposite structure. The dem-MWCNT/PMMA showed better dispersion of nanofiller than the raw-MWCNT in PMMA matrix. Agglomeration, i.e., localized clustering, of dem-MWCNT leads to formation of clearly visible nanotube-rich and nanotube-poor region in nanocomposite (Fig. S3b). The cohesive interactions between nanoparticles lead to the formation of sparingly dispersible aggregates. On the contrary, functionalization of MWCNTs by dapsone significantly improves nanofiller distribution (Fig. S3c). In dapson-MWCNT/PMMA, an imperfect three-dimensional network of randomly distributed particle/aggregates (reinforcement points) of nanofiller in the polymer matrix can be noticed. The better dispersion of the dapson-MWCNT leads to an increased volume fraction of altered polymer near the nanotubes surface causing efficient stress transfer propagation to a larger volume fraction of reinforcement points, i.e., nanotubes filler.

In order to get further inside in morphological properties of prepared nanocomposites, TEM micrographs of the samples containing 1.0 wt% of raw and functionalized MWCNTs are shown in Fig. 11a–d. Agglomeration process of unmodified MWCNTs and unequal distribution inside polymer matrix can be noticed in Fig. 11a, while the sample with dem-MWCNT (Fig. 11b) shows network formation and infrequently crosslinked nanotubes in the nanotube-poor region. The preserved inherent structure of dem-MWCNT (closed ends of nanotubes) is evident. This fact is attributed to relatively mild conditions in which the cycloaddition reaction takes place. It appears that crosslinking of the dem-MWCNT inside polymer matrix is not enough to ensure mechanical reinforcement as it can dapsone modified MWCNTs used as nanofiller. Completely interwoven structure in the case of dapson-MWCNT/polymer sample (Fig. 11c) provides strong interfacial bonding essential for efficient load transfer. The TEM micrographs demonstrated slightly disturbed structure (open ends) of nanotubes modified with dapsone (Fig. 11c) and fluorescein isothiocyanate (Fig. 11d) due to applied modification procedure (oxidation in a mixture of concentrated acids). Random and uneven distribution of fid-MWCNT inside polymer matrix corresponds to formation of nanotube-rich and nanotube-poor region in nanocomposite sample.

AFM Analysis

AFM was used to study the surface topology of nanocomposite films. Nanocomposites containing 0.5 and 1.0 wt% of functionalized MWCNTs were recorded in order to estimate the orientation and distribution of nanofillers inside polymer matrix. Representative AFM images of studied nanocomposites are shown in Figs. 12 and 13.

AFM images of neat PMMA, nanocomposites containing 0.5 wt% of dem-MWCNT and 0.5% of fid-MWCNT are shown in Fig. 12. Flat surfaces of neat PMMA, 0.5% dem-MWCNT/PMMA, and 0.5% fid-MWCNT/PMMA film can be observed in Fig. 12a–c.

An AFM analysis of nanocomposite sample with 0.5 wt% dapson-MWCNT, shown in Fig. 13a, confirms the presence of individual nanotubes near to film surface (nanotube protrude clearly from the surface) and hardly detectable small aggregates. The nanonotube dapson-MWCNT partially incorporated inside PMMA with a approximate width of 160 nm is spotted. Addition of higher amounts of dapson-MWCNT (Fig. 13b), causes appearance of the horizontally oriented and aligned nanotubes at film surface. Although dapson-MWCNT protrude at film surface they are thickly coated with polymer. The dimensions of the marked nanotubes on polymer surface are in the

 DOI 10.1002/pc

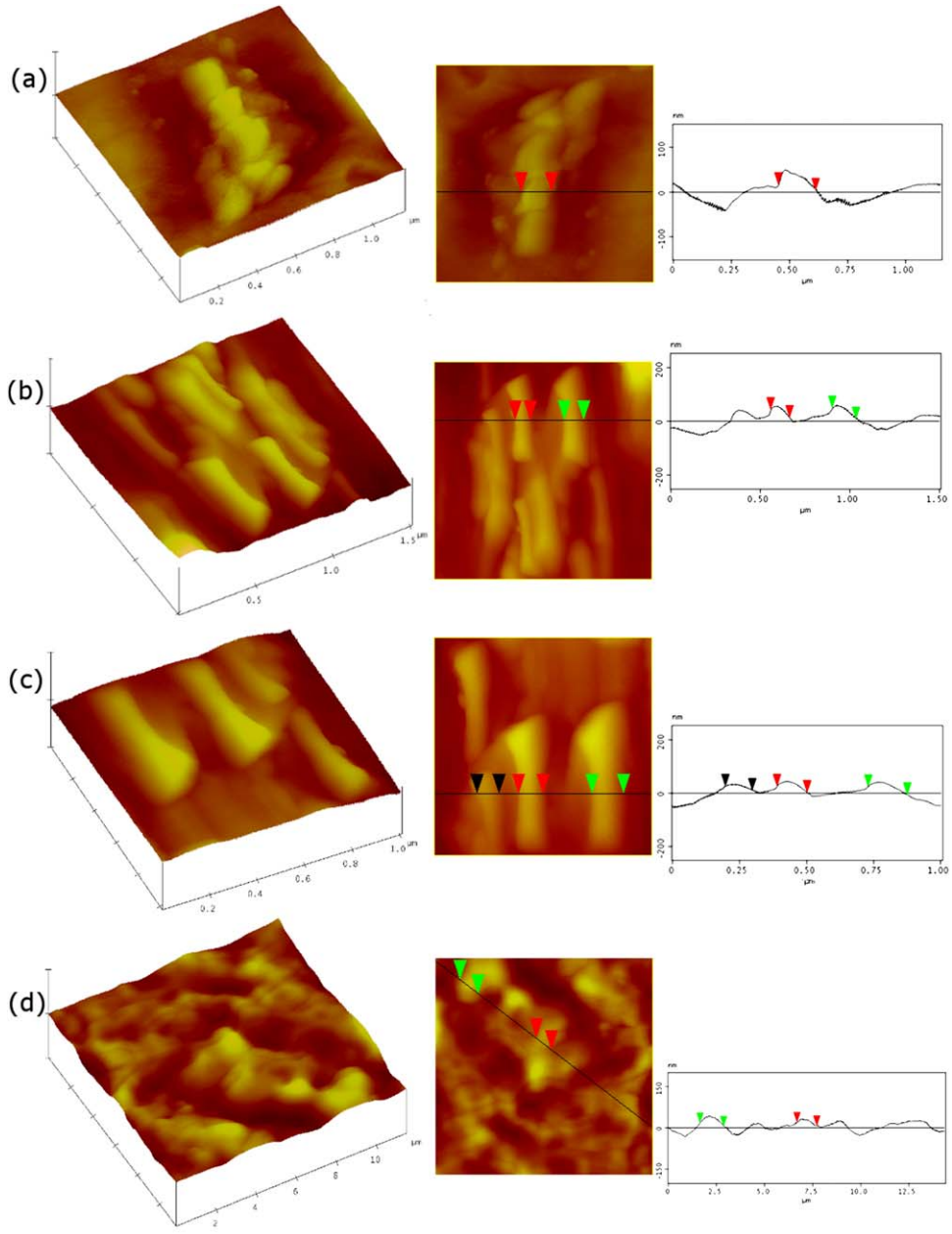

FIG. 13. 3D and 2D AFM images and height profiles of (a) 0.5% dapson-MWCNT/PMMA (1.2 × 1.2 × 0.2 μm), (b) 1% dapson-MWCNT/PMMA (1.5 × 1.5 × 0.5 μm), (c) magnified nanotubes from Fig. 13b (1 × 1 × 0.2 μm), and (d) 1% dem-MWCNT/PMMA (12 × 12 × 2 μm).

range of 130–180 nm. Figure 13c magnified selected area from Fig. 13b. From Fig. 13d, which shows nanocomposites with 1 wt% of dem-MWCNT, is not possible to spot individual nanotubes which implies that naonfiller is incorporated in polymer matrix. The widths marked in Fig. 13d are in the range from 1 to 1.5 μm, and smooth surface of the nanocomposite film containing 1 wt% of dem-MWCNT confirms this assumption. Addition of higher amounts than 2 wt% of all modified-MWCNTs results in an appearance of MWCNTs at film surface causing increase of surface roughness which prevents approach of the tip. Although surface chemistry of dem-MWCNT is relatively inert, the dapson-MWCNT contains pendant fragment which may create strong dipol/dipole and dipole/π-stacking interactions. Different polymer chain mobility due to geometric constrains and interfacial interaction at nanoparticle surface largely influenced on the properties of host polymer. Improved interfacial (mechanical) interlocking nanofiller/polymer chains provided better interaction/adhesion in dapson-MWCNT/PMMA nanocomposite.

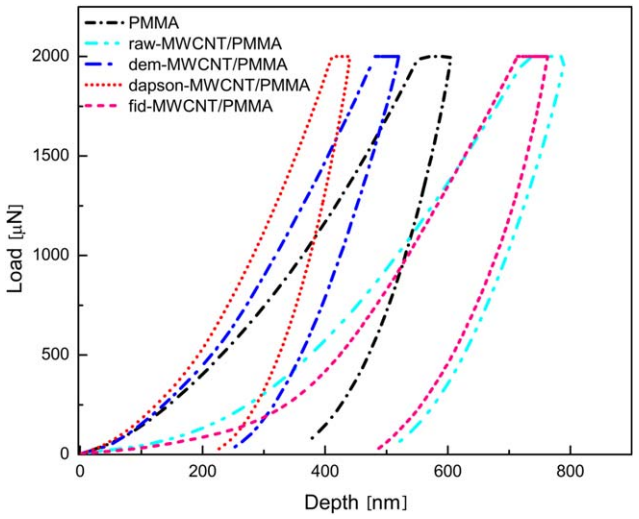

FIG. 14. Typical load-depth profiles for neat PMMA and nanocomposite samples with 1 wt% of raw-MWCNT and modified-MWCNT nanofiller.

Nanomechanical Characterization

The nanoindentation was used for studying nanomechanical properties, i.e., the reduced modulus and hardness, of neat PMMA and nanocomposite films. Typical load-depth profiles of the indents, recorded during the indentation of PMMA film and films with 1 wt% raw and functionalized MWCNTs are shown in Fig. 14. The steps and discontinuities on the plots were not observed, which implies that no cracks and fractures occurred during the nanoindentation measurements. The maximum indentation depth was measured for PMMA reinforced with raw-MWCNT. Nanocomposite containing fid-MWCNT also exhibited small resistance to the indentation load, while the largest resistance was obtained for the films loaded with dapson-MWCNT, while somewhat lower values was found for dem-MWCNT. After reaching the maximal indentation force, the plateau reveals the hold time of the indenter tip, which was predicted in order to minimize the polymer creep effect. The average hardness H and elastic modulus E of the modified-MWCNT/PMMA composite films, calculated using the Oliver-Pharr method [31], are listed in Table 4.

It can be observed that the hardness and elastic modulus of nanocomposite show the highest value for dapson-MWCNT/PMMA, which indicates existence of optimal interconnection (intensities of interfacial interaction) between polymer chains and functional groups on MWCNTs sidewalls. Addition of higher percentage of MWCNTs (>2 wt%) caused decrease in hardness and elastic modulus of all nanocomposites, indicating the best nanomechanical performance of samples containing 1 wt% of nanofiller. As example, value of reduced modulus for sample with 2 wt% of dapson-MWCNT slightly declined to 7.19 GPa, while for 4 wt% dramatically drop to 4.23 GPa. A maximum increase of 56% of reduced modulus and 86% of hardness was obtained for 1 wt% addition of dapson-MWCNT in PMMA.

TABLE 4. Average values of the reduced elastic modulus and the hardness of PMMA film and nanocomposite films with same MWCNTs content (1 wt%).

Sample	Reduced modulus (GPa)	Hardness (GPa)
PMMA	5.42 ± 0.17	0.320 ± 0.012
raw-MWCNT/PMMA	2.91 ± 0.13	0.165 ± 0.014
dem-MWCNT/PMMA	5.23 ± 0.19	0.504 ± 0.021
dapson-MWCNT/PMMA	8.47 ± 0.21	0.596 ± 0.019
fid-MWCNT/PMMA	3.65 ± 0.11	0.190 ± 0.011

Results of nanoindentation are in good accordance with T_g for nanocomposite loaded with raw-MWCNT and dapson-MWCNT, while some discrepancy was noticed for others. Such results indicate that mechanical properties of nanocomposite depends on chemical constitution, as well as configuration and conformation of the polymer phase, interactions between polymer chains, and degree of amorphousness. Also, the extent of interfacial and intermolecular interactions of polymer/nanofiller (hydrogen bonding, electrostatic, dipolar, Van der Vals interactions, etc.) depends on properties/number of functional groups present on polymer chains and the nanofiller surface.

Strong interfacial bonding between the matrix and the modified-MWCNTs is essential for achievement efficient load transfer which is reflected as high strength of nanocomposite under study. Plastic deformation in amorphous polymers occurs as a result of nucleation and propagation of shear bands [64]. In the unreinforced polymer matrix, shear bands propagate unhindered as there are no barriers for their movement. In contrast, the presence of modified-MWCNT in nanocomposites may be a resistance point for the propagation of shear bands [64]. Poor dispersion and high extent of aggregation, found for raw-MWCNT/PMMA (Fig. 11a), are due to hydrophobicity of raw-MWCNT surface. Imperfect interfacial adhesion and low wetting of raw-MWCNT by PMMA matrix are reflected in considerably by lower reinforcing effect. Introduction of dem-MWCNT produced an improvement in reinforcing effect indicating better compatibility with polymer matrix due to moderate dipolar interaction between ester group. In the case of dapson-MWCNT/PMMA, an existence a strong interfacial interaction between the matrix and the dapson-MWCNT nanosized reinforcement results in improved mechanical properties of the nanocomposite. A good mechanical interlocking and the increased obstacles to the motion of shear bands are the reasons for the enhancement of hardness and elastic modulus in dapson-MWCNT/PMMA nanocomposites. This result is in accordance with lower degree of amorphousness of nanocomposite, found by Raman and XRD analysis, and shift to higher T_g value, from DSC analysis, indicating significant strengthening in dapson-MWCNT-based nanocomposites. The further modification of terminal amino group in

DOI 10.1002/pc

dapsone molecule by attaching FITC, led to increase in aromaticity and voluminosity of resulting fid fragment in fid-MWCNT. Such a modification had a low effect on the polymer chain arrangement and reinforcement of fid-MWCNT/PMMA nanocomposites.

Correlation of the Obtained Experimental Results

This study aimed to investigate impact of nanofiller sidewalls functionalization on nanocomposite mechanical properties. Mammeri et al. [24] emphasized importance of MWCNTs controlled surface chemistry and its effect on nanomechanical properties of resulting composite films. We obtained substantial improvements in nanomechanical characteristics by adding lower amounts of modified MWCNTs by using simple preparation technique compared to conventional technology [24].

Structural properties of nanocomposites were thoroughly investigated in this study. FT-IR analysis did not provided substantial results only indicated the existence of noncovalent interaction in the system MWCNT/polymer. Intensive PMMA absorption bands completely overlapped the bands attributed to functionalized MWCNT in the cases of all prepared nanocomposites, resulting in a very similar, almost the same FT-IR spectra for all samples. XRD analysis reviled increase in a degree of amorphousness when high percentage of MWCNT was added. Particularly, XRD diffractogram of the nanocomposite sample containing 4 wt% of raw-MWCNT indicates existence of agglomeration process and aggregation of large amount of unmodified MWCNT into the bundles and consequentially, interaction between the tubes as a result of the unfavorable van der Waals forces. Those interactions causes decrease of the interfacial interaction between the polymer matrix and the MWCNTs, and therefore, increase in a degree of amorphousness of the nanocomposite sample.

The decrease in a degree of amorphousness of polymer matrix observed with loadings of 0.5 and 1 wt% dapson-MWCNT and dem-MWCNT, confirmed by Raman analysis and XRD spectroscopy contributes to improved mechanical performance. Nanocomposite sample containing 1 wt% of dem-MWCNT increased arrangement of polymer chains due to contribution of two important factors: appropriate degree of functionalization and optimal MWCNT concentration. We have previously demonstrated that introduction of diethyl malonate on the surface of MWCNT trough 1,3-dipolar cycloaddition does not causes disruption of inherent MWCNT properties [32]. Furthermore, the presence of diethyl malonate causes surface of MWCNT to retain its hydrophobic character and to be compatible with hydrophobic PMMA chains. At a concentration of 1 wt% dem-MWCNT optimal equilibrium interactions of diethyl malonate groups and PMMA enables a good distribution of filler. Higher concentration of dem-MWCNT inside polymer prevailed hydrophobic forces among diethyl malonate molecules on MWCNT sidewalls and causes stronger interactions among nanotubes itself rather than between diethyl malonate groups and PMMA matrix. Increasing the MWCNTs concentration up to a certain level provides optimal polymer/MWCNT contact homogeneity. An appropriate level of interfacial stress transfer, reflected in terms of improved mechanical properties was achieved.

Addition of 1 wt% of dapson-MWCNT promotes optimal conformation of the polymer chains and therefore, the best reinforcement for the PMMA. Dapsone moiety ameliorated the compatibility between polymer phase and MWCNT surface. The displayed behavior can be explained by the nature of the functional groups present on the surface of the dapson-MWCNTs: dipole/π-stacking attractive interaction between phenyl moieties and polymer chain provides a higher extent of intermolecular interactions in highly ordered nanophases, contributing to effective networking of the system. The increase of the binding energy/affinity of a small-molecule (moieties) was a consequence of the present substituent (group) at phenyl rings. The phenyl group had no dipole moment, but instead presence of sulfonyl group caused formation of a positive charge on the atoms in the ring and a correspondingly negative charge (π-delocalized electronic cloud) above and below the ring. Electron-withdrawing groups, i.e., sulfonyl group, reduced the negative quadropole of the aromatic ring and thereby favored parallel displaced and sandwich conformations. Contrastingly, electron donating groups, i.e., amino group, increased the negative quadropole, which can increase the interaction strength in a T-shaped configuration with the proper geometry. Electronic structures of these two phenyl rings provided conditions for intensive dipole/π-stacking attractive interaction. On the other hand, low intensity noncovalent interactions: London dispersive forces, Van der Vaals, and different dipolar interactions had a smaller contribution to orderliness and physical crosslinking of the system dem-MWCNT/PMMA, contributing to lower nanomechanical properties. The obtained results show that aromatic-functionalization with a proper geometrical design of attached moiety may be a key factor in a novel design of nanocomposite with improved nanofiller dispersion, and creation of strong interfacial bonding between nanofiller and matrix causing improved hardness and reduced modulus of nanocomposites. A further increase of the MWCNTs content (>1 wt%) induces agglomeration of nanofiller and weakening of noncovalent filler-polymer interaction. These defects, caused by prevailing nanotube-nanotube forces lead to formation of the internal cavities and disrupt composite structure integrity. Formation of the internal cavities and decrease in homogeneity of the composite resulted in a reduction of composite nanomechanical performance.

CONCLUSIONS

The modified-MWCNT/PMMA nanocomposites have been fabricated by solution casting technique in a form of

thick free standing films. Functionalization of MWCNTs sidewalls promoted compatibility between the polymer matrix and filler nanoparticles. The decrease in a degree of amorphousness of polymer matrix with loadings of 0.5 and 1 wt% dapson-MWCNT and dem-MWCNT is confirmed by Raman analysis and XRD spectroscopy. SEM and TEM microscopy provided information on MWCNTs distribution within nanocomposite samples. Orientation of individual MWCNTs on the surface of nanocomposite films was analyzed by AFM microscopy. Improvements in thermal properties were attributed to the well dispersion of functionalized MWCNTs within polymer matrix due to functionalization, i.e., compatibility of nanofiller and PMMA matrix. Furthermore, enhancement in nanomechanical properties of nanocomposites containing 1 wt% of dem-MWCNT and dapson-MWCNT implies that those functionalities contributed to compatibility and enabled to some extent of ordered arrangement among the polymer chains. The presented results demonstrated that suitable sidewall functionalization (interface chemistry) and nanoscale morphology at appropriate nanofiller loading can improve thermal stability and nanomechanical properties of well design nanocomposites.

REFERENCES

1. H.X. Wu, X.Q. Qiu, W.M. Cao, Y.H. Lin, R.F. Cai, and S.X. Qian, *Carbon*, **45**, 2866 (2007).
2. A.K. Singh, *Indian J. Pure Appl. Phys.*, **51**, 439 (2013).
3. D. Shao, J. Hu, Z. Jiang, and X. Wang, *Chemosphere*, **82**, 751 (2011).
4. S.M. Yuen, C.C.M. Ma, C.Y. Chuang, K.C. Yu, S.Y. Wu, C.C. Yang, and M.H. Wei, *Compos. Sci. Technol.*, **68**, 963 (2008).
5. N.K. Shrivastava, P. Kar, S. Maiti, and B.B. Khatua, *Polym. Int.*, **61**, 1683 (2012).
6. Y. Zheng, J. Zhang, Y. Xiaodong, W. Chen, and R. Wang, *J. Appl. Polym. Sci.*, **112**, 1755 (2009).
7. W. Zhong and J.P. Claverie, *Carbon*, **51**, 72 (2013).
8. B. Sundaray, V. Subramanian, T.S. Natarajan, and K. Krishnamurthy, *Appl. Phys. Lett.*, **88**, 143114 (2006).
9. H.J. Choi, K. Zhang, S.Y. Park, and B.Y. Lee, *J. Nanosci. Nanotechnol.*, **9**, 6089 (2009).
10. C. McClory, T. McNally, M. Baxendale, P. Pötschke, W. Blau, and M. Ruether, *Eur. Polym. J.*, **46**, 854 (2010).
11. E. Logakis, C. Pandis, P. Pissis, J. Pionteck, and P. Potschke, *Compos. Sci. Technol.*, **71**, 854 (2011).
12. G.T. Pham, Y.B. Park, Z. Liang, C. Zhang, and B. Wang, *Compos. Part B*, **39**, 209 (2008).
13. M.A. Pantoja-Castro, J.F. Pérez-Robles, H. González-Rodríguez, Y. Vorobiev-Vasilievitch, H.V. Martínez-Tejada, and C. Velasco-Santos, *Mater. Chem. Phys.*, **140**, 458 (2013).
14. H. Jung, S.Y. An, D.M. Jang, J.M. Kim, J.Y. Park, and D. Kim, *Carbon*, **50**, 987 (2012).
15. P.G. Su and C.S. Wang, *Sens. Actuators B*, **124**, 303 (2007).
16. A. Martinez, S. Uchida, Y.W. Song, T. Ishigure, and S. Yamashita, *Opt. Express*, **16**, 11337 (2008).
17. B. Philip, J.K. Abraham, A. Chandrasekhar, and V.K. Varadan, *Smart Mater. Struct.*, **12**, 935 (2003).
18. M. Lahelin, M. Annala, A. Nykänen, J. Ruokolainen, and J. Seppälä, *Compos. Sci. Technol.*, **71**, 900 (2011).
19. A.K. Pradhan and S.K. Swain, *J. Mater. Sci. Technol.*, **28**, 391 (2012).
20. F. Pourfayaz, A.A. Khodadadi, Y. Mortazavi, and S.H. Jafari, *Plasma Processes Polym.*, **7**, 1001 (2010).
21. H. Roghani-Mamaqani, V. Haddadi-Asl, M. Ghaderi-Ghahfarrokhi, and Z. Sobhkhiz, *Colloid Polym. Sci.*, **292**, 2971 (2014).
22. J.N. Shen, C.C. Yu, H.M. Ruan, C.J. Gao, and B. Vander Bruggen, *J. Membr. Sci.*, **442**, 18 (2013).
23. F. Mammeri, J. Teyssandier, C. Darche-Dugaret, S. Debacker, E.L. Bourhis, and M.M. Chehimi, *J. Colloid Interface Sci.*, **433**, 115 (2014).
24. F. Mammeri, J. Teyssandier, C. Connan, E. Le Bourhis, and M.M. Chehimi, *R. Soc. Chem. Adv.*, **2**, 2462 (2012).,
25. H. Chakraborty, A. Sinha, N. Mukherjee, D. Ray, and P. Protim Chattopadhyay, *Polym. Compos.*, **35**, 948 (2014).
26. J.T. Luo, H.C. Wen, W.F. Wu, and C.P. Chou, *Polym. Compos.*, **29**, 1285 (2008).
27. P. Slobodian, A. Lengálová, and P. Sáha, *J. Reinf. Plast. Compos.*, **26**, 1705 (2007).
28. S. Kim, Y.I. Lee, D.H. Kim, K.J. Lee, B.S. Kim, M. Hussain, and Y.H. Choa, *Carbon*, **51**, 346 (2013).
29. G. Tripathi, B. Tripathi, Y.K. Vijay, A. Chandra, and M.K. Sharma, *Int. J. Chem. Sci.*, **9**, 1725 (2011).
30. G.D. Vuković, S.Z. Tomić, A.D. Marinković, V. Radmilović, P.S. Uskoković, and M. Čolić, *Carbon*, **48**, 3066 (2010).
31. W.C. Oliver and G.M. Pharr, *J. Mater. Res.*, **7**, 1564 (1992).
32. D. Brković, M.L. Avramov Ivić, V.M. Rakić, L. Valentini, P.S. Uskoković, and A.D. Marinković, *J. Phys. Chem. Solids*, **83**, 121 (2015).
33. S. Zhou, Y. Yin, B. You, L. Wu, and M. Chen, *Macromol. Chem. Phys.*, **208**, 2677 (2007).
34. Z.L. Xie, H.B. Xu, A. Geßner, M.U. Kumke, M. Priebe, K.M. Fromm, and A. Taubert, *J. Mater. Chem.*, **22**, 8110 (2012).
35. A. Singhal, K.A. Dubey, Y.K. Bhardwaj, D. Jain, S. Choudhury, and A.K. Tyagi, *R. Soc. Chem. Adv.*, **3**, 20913 (2013).
36. R. Hussain and D. Mohammad, *Turk. J. Chem.*, **28**, 725 (2004).
37. E. Shobhana, *IJMER*, **2**, 1092 (2012).
38. G. Vuković, A. Marinković, M. Obradović, V. Radmilović, M. Čolić, R. Aleksić, and P.S. Uskoković, *Appl. Surf. Sci.*, **255**, 8067 (2009).
39. A. Cao, C. Xu, J. Liang, D. Wu, and B. Wei, *Chem. Phys. Lett.*, **344**, 13 (2001).
40. M. Salami-Kalajahi, V. Haddadi-Asl, F. Behboodi-Sadabad, S. Rahimi-Razin, and H. Roghani-Mamaqani, *Polym. Compos.*, **33**, 215 (2012).
41. W. Guojian, Q. Zehua, L. Lin, S. Quan, and G. Jianlong, *Mater. Sci. Eng. A*, **472**, 136 (2008).

42. L. Zeng, W. Wang, J. Liang, Z. Wang, Y. Xia, D. Lei, X. Ren, N. Yao, and B. Zhang, *Mater. Chem. Phys.*, **108**, 82 (2008).
43. D. Shao, Z. Jiang, X. Wang, J. Li, and Y. Meng, *J. Phys. Chem. B*, **113**, 860 (2009).
44. C. Chen, B. Liang, A. Ogino, X. Wang, and M. Nagatsu, *J. Phys. Chem. C*, **113**, 7659 (2009).
45. C. Chen, A. Ogino, X. Wang, and M. Nagatsu, *Appl. Phys. Lett.*, **96**, 131504 (2010).
46. C. Chen, B. Liang, A. Ogino, X. Wang, and M. Nagatsu, *Carbon*, **48**, 939 (2010).
47. D. Shao, J. Hu, C. Chen, G. Sheng, X. Ren, and X. Wang, *J. Phys. Chem. C*, **114**, 21524 (2010).
48. S. Costa, E. Borowiak-Palen, M. Kruszynska, A. Bachmatiuk, and R.J. Kalenczuk, *Mater. Sci. Poland*, **26**, 433 (2008).
49. A. Jorio, M.A. Pimenta, A.G. Souza Filho, G.G. Samsonidze, A.K. Swan, M.S. Ünlü, B.B. Goldberg, R. Saito, G. Dresselhaus, and M.S. Dresselhaus, *Phys. Rev. Lett.*, **90**, 107403 (2003).
50. M.S. Dresselhaus, G. Dresselhaus, R. Saito, and A. Jorio, *Phys. Rep.*, **409**, 47 (2005).
51. N. Soin, S.S. Roy, S.C. Ray, and J.A. McLaughlin, *J. Raman Spectrosc.*, **41**, 1227 (2010).
52. A. Jorio, M.A. Pimenta, A.G. Souza Filho, G. Dresselhaus, M.S. Dresselhaus, and R. Saito, *New J. Phys.*, **5**, 139 (2003).
53. G. Wu and J. Dong, *Phys. Rev. B*, **73**, 245414 (2007).
54. V. Datsyuk, M. Kalyva, K. Papagelis, J. Parthenios, D. Tasis, A. Siokou, I. Kallitsis, and C. Galiotis, *Carbon*, **46**, 833 (2008).
55. M. Zdrojek, W. Gebicki, C. Jastrzebski, T. Melin, and A. Huczko, *Solid State Phenom.*, **99**, 1 (2004).
56. E.F. Antunes, A.O. Lobo, E.J. Corat, and V.J. Trava-Airoldi, *Carbon*, **45**, 913 (2007).
57. A.M. Rao, A. Jorio, M.A. Pimenta, M.S.S. Dantas, R. Saito, G. Dresselhaus, and M.S. Dresselhaus, *Phys. Rev. Lett.*, **84**, 1820 (2000).
58. L. Bokobza, *Polym. Adv. Technol.*, **23**, 1543 (2012).
59. H. Murphy, P. Papakonstantinou, and T.I.T. Okpalugo, *J. Vac. Sci. Technol. B*, **24**, 712 (2006).
60. S. Reich and C. Thomsen, *Philos. Trans. R. Soc. Lond. Ser. A*, **362**, 2271 (2004).
61. I. Abdullahi, N. Sakulchaicharoen, and J.E. Herrera, *Diamond Relat. Mater.*, **23**, 76 (2012).
62. T. Hatakeyama and F.X. Quinn, *Thermal Analysis: Fundamentals and Applications to Polymer Science*, 2nd ed., Wiley, England (1999).
63. A. Zanotto, A.S. Luyt, A. Spinella, and E. Caponetti, *Eur. Polym. J.*, **49**, 61 (2013).
64. B. Das, K.E. Prasad, U. Ramamurty, and C.N.R. Rao, *Nanotechnology*, **20**, 125705 (2009).